

A Catalog of M-dwarf Flares with ASAS-SN

ROMY RODRÍGUEZ MARTÍNEZ,¹ LAURA A. LOPEZ,^{1,2,3} BENJAMIN J. SHAPPEE,⁴ SARAH J. SCHMIDT,⁵
THARINDU JAYASINGHE,¹ CHRISTOPHER S. KOCHANÉK,¹ KATIE AUCHETTL,^{6,7} AND THOMAS W.-S. HOLOIEN^{8,*}

¹*Department of Astronomy, The Ohio State University, 140 W. 18th Ave., Columbus, Ohio 43210, USA*

²*Center for Cosmology and AstroParticle Physics, The Ohio State University, 191 W. Woodruff Ave., Columbus, OH 43210, USA*

³*Niels Bohr Institute, University of Copenhagen, Blegdamsvej 17, 2100 Copenhagen, Denmark*

⁴*Institute for Astronomy, University of Hawai'i, 2680 Woodlawn Drive, Honolulu, HI 96822, USA*

⁵*Leibniz-Institute for Astrophysics Potsdam (AIP), An der Sternwarte 16, 14482, Potsdam, Germany*

⁶*DARK, Niels Bohr Institute, University of Copenhagen, Lyngbyvej 2, 2100 Copenhagen, Denmark*

⁷*Department of Astronomy and Astrophysics, University of California, Santa Cruz, CA 95064, USA*

⁸*The Observatories of the Carnegie Institution for Science, 813 Santa Barbara St., Pasadena, CA 91101, USA*

Submitted to ApJ

ABSTRACT

We analyzed the light curves of 1376 early-to-late, nearby M dwarfs to search for white-light flares using photometry from the All-Sky Automated Survey for Supernovae (ASAS-SN). We identified 480 M dwarfs with at least one potential flare employing a simple statistical algorithm that searches for sudden increases in *V*-band flux. After more detailed evaluation, we identified 62 individual flares on 62 stars. The event amplitudes range from $0.12 < \Delta V < 2.04$ mag. Using classical-flare models, we place lower limits on the flare energies and obtain *V*-band energies spanning $2.0 \times 10^{30} \lesssim E_V \lesssim 6.9 \times 10^{35}$ erg. The fraction of flaring stars increases with spectral type, and most flaring stars show moderate to strong H α emission. Additionally, we find that 14 of the 62 flaring stars are rotational variables, and they have shorter rotation periods and stronger H α emission than non-flaring rotational variable M dwarfs.

Keywords: stars: activity – stars: flare – stars: late-type – stars: low-mass

1. INTRODUCTION

Stellar flares are the consequence of surface magnetic fields. When magnetic field lines reconnect, they cause large, rapid flux increases in the UV, X-ray and sometimes optical wavelengths (France et al. 2013; Jones & West 2016; Hawley et al. 2014). Flares, sunspots and prominences, as well as other magnetic phenomena, have been extensively studied since the mid-1800s after the Carrington Event on the Sun (Carrington 1859). Subsequent studies of starspots, flare activity have been extended down to the low-mass end of the main sequence (e.g., Hawley et al. 1996; Kowalski et al. 2013; Hawley et al. 2014; Newton et al. 2016; Mondrik et al. 2018; Yang et al. 2017; Günther et al. 2019). Photometric ob-

servations of M dwarfs, cool and small stars with temperatures and masses between 2400–4000 K and 0.2–0.63 M_{\odot} , respectively (Gershberg 2005), reveal strong chromospheric activity with starspots and flares and activity lifetimes that persist over Gyr timescales, longer than on Sun-like stars (West et al. 2008).

Some open issues in stellar physics and activity include the evolution of the magnetic field strength and whether low-mass stars exhibit activity cycles like those observed in the Sun and Sun-like stars (Vida et al. 2013, 2014). Additionally, the dependence of flare rates on spectral type and age has not been fully characterized (Ilin et al. 2018). Previous studies suggest that M4 and later-type stars flare with higher frequency and larger amplitudes than earlier M stars (Kowalski et al. 2009; Davenport et al. 2012; Hawley et al. 2014). However, very low-mass stars ($< 0.35 M_{\odot}$) are typically convective and lack tachoclines (Chabrier & Baraffe 1997), which

Corresponding author: Romy Rodríguez Martínez
rodriguezmartinez.2@osu.edu

* Carnegie Fellow

raises questions about the drivers of heightened activity in the very low-mass regime.

Other questions in stellar and flare physics involve the relationships between activity, ages and rotation rates. There is evidence that rapid rotators are more active than slow rotators (Kiraga & Stepien 2007; Newton et al. 2017; Mondrik et al. 2018), but identifying and studying flares and activity cycles requires long-term observations of these stars. With the advent of large surveys like the All-Sky Automated Survey (ASAS; Pajmanski 1997), Evryscope (e.g., Howard et al. 2019), the Panoramic Survey Telescope and Rapid Response System (Pan-STARRS; Kaiser 2004), the *Kepler* Space Telescope (Borucki et al. 2010), the Transiting Exoplanet Survey Satellite (*TESS*; Ricker et al. 2015), and the All-Sky Automated Survey for Supernovae (ASAS-SN; Shappee et al. 2014; Kochanek et al. 2017), it has been possible to obtain detailed observations of flares across a wide range of spectral types and wavelengths, allowing some of these questions to be answered. However, our understanding of the rates and energy distributions of flares on M dwarfs is not complete, and an in-depth exploration of M-dwarf activity requires more observations. This is especially true in the very low-mass regime, where observations are more challenging because the stars are optically faint.

Here we search for flares from M-dwarf stars in ASAS-SN. ASAS-SN is an all-sky, optical survey with the primary goal of identifying bright supernovae and other transients. ASAS-SN presently consists of twenty 14-cm telephoto lenses, covering around 16000 sq. degrees at a median cadence of roughly 21 hours in g band and $\sim 2\text{--}3$ days in V band from 2012 to 2018 (the time span considered in this paper).

Several strong flares have been found with ASAS-SN (Stanek et al. 2013; Simonian et al. 2016; Rodríguez et al. 2018) and characterized in detail (Schmidt et al. 2014, 2016). Recently, Schmidt et al. (2018) compiled a catalog of M-dwarf flares serendipitously identified in the first four years of ASAS-SN transient alerts. Schmidt et al. (2018) followed-up these events with additional photometry and spectroscopy of the host stars.

The study of flares and stellar activity of M dwarfs is important for the habitability of planets orbiting these small, cool stars. Transit and radial velocity exoplanet missions have uncovered an abundance of small planets in the habitable zones of M dwarfs (e.g., Dressing & Charbonneau 2015), making them crucial targets in the search for habitable worlds. However, planets in the habitable zones of M dwarfs are more exposed to stellar activity, including strong X-ray and UV emission from flares, because the habitable zones are only ~ 0.1

AU from the star. As such, the activity of these stars is important because planetary habitability depends on both intrinsic planet properties and the characteristics of their host stars.

Although previous studies suggest that stellar activity negatively affects planetary atmospheres and potential surface life, the details remain an open question (e.g., Segura et al. 2010; Davenport 2016; Vida et al. 2017; O’Malley-James & Kaltenegger 2019). Recent observations of strong and frequent flares in the mid-M dwarf Proxima Centauri have raised doubts about the existence of an atmosphere and therefore the habitability of its Earth-mass exoplanet (Davenport 2016; Howard et al. 2018). There is significant evidence suggesting that magnetic activity and flares can cause atmospheric erosion (Lammer et al. 2007), runaway greenhouse effects, and hydrodynamic escape of the atmospheres (Luger & Barnes 2015; Shields et al. 2016).

Large-scale studies of activity and flares on nearby, planet-bearing M dwarfs of all spectral types will allow prioritization of systems for follow-up observations with James Webb Space Telescope (*JWST*) and other upcoming missions. Stars with low-activity are more promising targets for *JWST* if the aim is to find habitable exoplanets. Detailed observations of active planet hosts can reveal how activity affects planet atmospheres, and probe other relevant problems, like the interaction between stellar and planetary magnetic fields (e.g., Poppenhaeger 2015).

Flares are unpredictable transients, so a systematic study of flares requires frequent observations over extended periods of time. In this paper, we examine two samples of M dwarfs using ASAS-SN. We search for flares in the magnitude-limited sample of earlier M-dwarfs from Lépine et al. (2013) and in the volume-limited (< 20 pc) sample of later M-dwarfs from Cruz et al. (2007). After identifying flares, we investigate the correlations between flare frequency, flare energy, spectral type and $H\alpha$ as a stellar activity indicator.

The structure of this paper is as follows. In Section 2, we describe the sample and our methodology to identify flares. We also discuss the potential sources of false positives and completeness. In Section 3.1, we estimate the energies of the identified flares, and in Section 3.2, we identify rotational variables in our sample and measure their rotational periods. In Section 3.3, we note which candidates in our sample host confirmed or potential exoplanets. Finally, in Section 4, we summarize our results.

2. OBSERVATIONS AND DATA ANALYSIS

2.1. The Sample

Table 1. Spectral types for the stars in our sample

spt	Lépine et al. (2013)	Cruz et al. (2007)
M0	337	-
M1	299	1
M2	260	1
M3	250	2
M4	108	1
M5	18	11
M6	2	20
M7	1	31
M8	1	18
M9	-	10

The majority of the sources we analyzed were taken from the Lépine et al. (2013) sample of bright M dwarfs. Lépine et al. (2013) is a spectroscopic, magnitude-limited catalog of the brightest ($J < 9$ mag) late-K and M dwarfs in the Northern hemisphere. It is comprised of 1564 sources, of which 1408 are spectroscopically confirmed to be stars between K7 and M6 in spectral type. This catalog is estimated to contain $\sim 90\%$ of all M dwarfs in the North with $J < 9$ mag and they have a mean V -band brightness of $V \sim 12$ mag. The spectral classifications have an estimated precision of a half-subtype. The dwarf classifications require proper motions of $\mu > 40$ mas yr $^{-1}$ to exclude red giants. We used only the sources with reliable spectral classifications, leading to a total of 1276 objects between M0 and M8 (see Table 1).

Lépine et al. (2013) estimated the effective temperatures of these stars by fitting their spectra with PHOENIX atmospheric models (Allard et al. 2011). They also identified active M dwarfs based on their H α features. The strength of this line is a standard diagnostic of chromospheric activity in M dwarfs, with the most active M dwarfs showing H α in emission rather than absorption, although some active late-K and early M dwarfs can also show H α in absorption (Walkowicz & Hawley 2009; Newton et al. 2017). These M dwarfs have $2660 \text{ K} < T_{\text{eff}} < 3940 \text{ K}$ and a typical H α equivalent width of -3 \AA .

We complement these sources with a volume-limited (< 20 pc) sample of late-M and ultracool dwarfs identified from 2MASS by Cruz et al. (2007). The Lépine et al. (2013) and Cruz et al. (2007) samples are different and do not overlap. As with the Lépine et al. (2013) sample, we only use the objects spectroscopically classified as M

dwarfs, yielding a sample of 100 M dwarfs with spectral types between M1–M9 (see Table 1), of which 97% are M5 or later. These sources have typical V -band magnitudes of $V \sim 16$ mag. The stars from both catalogs were selected without reference to H α emission or other classifiers of magnetic activity, so the sample includes both active and inactive stars.

Although we did not use this information while vetting the candidates, there is external data on the activity of these stars. In Simbad (Wenger et al. 2000) and the International Variable Stars Index (VSX, Watson et al. 2006), 122 are identified as flare stars, generally UV Ceti stars which show flares with $\Delta V \simeq 0.1$ to $\Delta V \simeq 6$ mag. The others with flare star designations in Simbad come from a sample of ~ 570 stars flagged in the GALEX all-sky UV survey (Jones & West 2016) because they have excess UV emission.

2.2. The All-Sky Automated Survey for Supernovae (ASAS-SN)

After selecting the candidates, we obtained ASAS-SN aperture photometry for each of the 1376 stars, and we modified the standard ASAS-SN photometry pipeline to account for proper motions of the M dwarfs. Prior to 2018, ASAS-SN consisted of 4 telescopes monitoring the sky every 2–3 days to $V \simeq 17$. Afterwards, it rapidly built up to 20 telescopes monitoring the sky every 21 hours to $g \simeq 18$. ASAS-SN takes 3 dithered 90-second exposures, and we obtained the light curves for these individual exposures rather than the sum. ASAS-SN has magnitude limits of $V \approx 16.5 - 17.3$ and $g \approx 18$ and photometric precision of ~ 0.02 mag at $V \sim 12$ mag and ~ 0.08 mag at $V \sim 16$ mag (Jayasinghe et al. 2018).

One disadvantage of ASAS-SN is that its cadence is low and the integration time of 90 seconds is short relative to the timescale of a flare (~ 100 seconds; Davenport 2016). This limits both the number of detections of a given flare, as well as the number of observable flares from each star. The former means that the shape or morphology of the flare, with its characteristic fast rise and slower exponential decay, is not well constrained. This is a limitation compared to large-scale flare searches on M dwarfs with high-cadence photometry using, for example, *Kepler*/K2 (Davenport 2016; Doyle et al. 2018) or Evryscope (Howard et al. 2018, 2019).

2.3. Flare identification

In order to identify flares, we searched all of the M-dwarf light curves to select the sources with potential flares. We computed the mean, V_{mean} , median V_{median} , and standard deviation σ of each light curve. We then

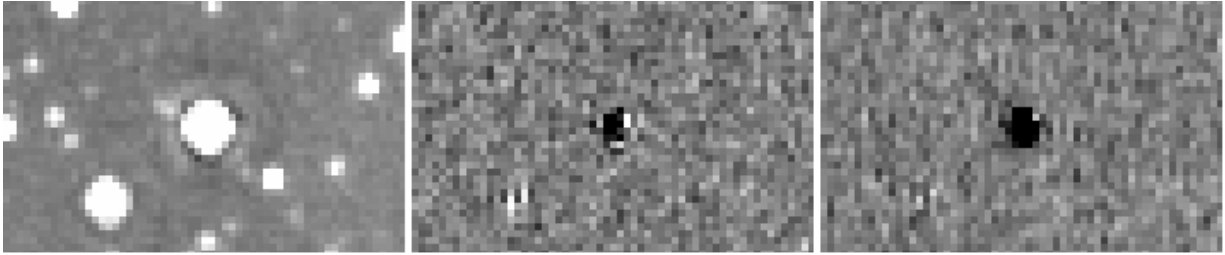


Figure 1. A $\Delta V = 0.14$ mag flare on the early-M star I04480+1703. The target lies at the center of each image. The image on the **left** is the ASAS-SN reference image of the star, while the **middle** and **right** images are the difference between the reference and two images at the epoch of flare.

identified positive magnitude excursions that were $> 2\sigma$ from the light curve and selected events that satisfied

$$\frac{V_{\text{peak}} - V_{\text{median}}}{\sigma} \geq 2 \quad (1)$$

where V_{peak} is the peak magnitude of the flare. We used the median rather than the mean because the former is less sensitive to outliers. We chose a statistical cut of 2σ , in contrast to other works who use slightly higher cuts (e.g., Kowalski et al. 2009 and Hawley et al. 2014 use 3σ and 2.5σ , respectively) to try to identify smaller flux increases.

Many of the $\geq M5$ stars in the Cruz et al. (2007) sample are not directly detected by ASAS-SN and have light curves that largely consist of upper limits. For these stars we define a median magnitude based on the number of upper limits and good detections. If a light curve consisted only of upper limits, we discarded it, regardless of whether it had statistically significant outliers, as upper limits are not reliable enough for the confirmation of flares. If the light curve had a combination of upper limits and detections, then we took the median of the entire light curve. Finally, if it consisted of mostly detections (i.e., not upper limits), then we only considered the detection median rather than the median on the entire light curve.

After applying these criteria, we had 556 stars with at least one candidate flare in the Lépine et al. (2013) sample and 27 in the Cruz et al. (2007) sample. Many of these candidates were false positives from 2012 when ASAS-SN had just started, so we dropped this early data. We also excluded saturated stars (with $V < 10$ mag) since the corrections for saturation in the ASAS-SN pipeline (see Kochanek et al. 2017) are not reliable. After rejecting images taken in bad weather, with $\text{FWHM} \geq 2.5$ pixels (71 candidates) and saturated stars (32 candidates), 453 stars with candidate flares were left from Lépine et al. (2013) and 27 from Cruz et al. (2007).

Next, we inspected the light curves to confirm or discard the candidates. In particular, we examined the subtracted images of the candidate flares. If the flare

candidate is real, the subtracted image should show a negative, star-like image at the location of the source, such as that shown in Figure 1. In general, we kept flares that had at least 2 consecutive, $> 2\sigma$ detections of the flare and a clear signal in the subtraction images at the time of the flare. In ~ 10 cases, we kept flares with only one $\geq 2\sigma$ detection because the signal in the subtracted image was strong and clean.

Consecutive points that were marginally above the threshold (i.e., a few millimag above the threshold) were not considered as flares because they likely result from some systematic problem. We also verified that the flare durations of the putative events were consistent with the durations of well-studied classical (singly-peaked) flares. Almost all observed M-dwarf flares have durations of less than 90 minutes (Hawley et al. 2014), although there are exceptions (e.g., Kowalski et al. 2010). None of the flares identified in our sample had durations of more than 90 minutes.

We assume that all confirmed events are classical flares rather than a mixture of classical and complex (multi-peaked structures; see e.g., Hawley et al. (2014) for a discussion of classical and complex flares). Although this assumption is not necessarily true, ASAS-SN does not have the photometric precision and cadence to resolve multi-peaked events, especially since these can last longer than classical flares (up to ~ 8 -12 hours, e.g., Kowalski et al. 2010).

At the end of the validation process, we had a final sample of 62 stars with at least one flare in the Lépine et al. (2013) sample. We could not confirm any of the candidates in the Cruz et al. (2007) sample. Most of these stars are near the detection limit of ASAS-SN ($V \approx 16.5 - 17.3$ mag), undetected in their quiescent state and with only a single detection during the putative flare. The flare images for these sources were also not of high quality compared to those from the Lépine et al. (2013) sample. Consequently, the data were only sensitive to rarer, higher amplitude flares from a small number of stars.

We designate 8 flares as “Maybes”, where the candidates could not be confirmed (see Table 3). A few of these are from the early (< 2013) phase of ASAS-SN, when systematic issues were less well controlled.

3. RESULTS

We identified 62 flares on 62 stars from the [Lépine et al. \(2013\)](#) sample. Figure 2 shows a few representative light curves, and Table 3 contains the properties of these stars. Of these, 34 were stars with previously observed flares, but the remaining 28 ($\sim 45\%$) are new. The 34 on known flare stars are 27% of the 122 in the sample, which gives a very rough sense of the “completeness”. In practice, flare energies follow a power-law distribution, so completeness is a complex combination of the duty cycle of the observations, individual flare rates, and our amplitude sensitivity, so this should only be interpreted qualitatively.

The flaring candidates range in spectral types between early M0 to M5 with temperatures of 2850 K to 3730 K. Their average distance is 62 pc (as inferred from [Bailer-Jones et al. 2018](#)), and they have a median quiescent brightness of $V = 12.6$ mag. These stars may have flared multiple times over the duration of the ASAS-SN observations (~ 6 years), and visual inspection of the light curves indeed reveals several small events that passed the statistical cut. The amplitudes of most of the events are small, only a fraction of a magnitude. Specifically, they range from $0.12 < \Delta V < 2.04$ mag. We list the ΔV and the energies (Section 3.1) of the highest-amplitude events of each star, and include the number of potential flares in their light curves (events that passed the statistical threshold but were not confirmed) in Table 4.

Figure 3 shows a histogram of all the stars with confirmed flares binned by spectral type from M0 to M5. The fraction of stars by spectral type with confirmed flares rises from M1 to M5, peaking at 25% for M5, consistent with previous studies of M-dwarf flares ([Kowalski et al. 2009](#); [Yang et al. 2017](#); [Mondrik et al. 2018](#); [Günther et al. 2019](#)). [Yang et al. \(2017\)](#) identified 540 M dwarfs with flares from *Kepler* long-cadence data and discovered that the active fraction rises steeply near the M4 subtype, coinciding with the threshold at which M dwarfs become fully convective. [Günther et al. \(2019\)](#) found a similar trend from a systematic study of 763 flaring M stars in *TESS* ranging from M0 to M8, with flare activity peaking for the M5 stars. Additionally, [West et al. \(2004\)](#) examined 8000 late-type dwarfs in the Sloan Digital Sky Survey using the $H\alpha$ emission line as an activity indicator, and they showed that the fraction of active stars peaks near M8, in agreement with past work ([Hawley et al. 1996](#); [Gizis et al. 2000](#); [Kowalski](#)

[et al. 2009](#); [Schmidt et al. 2016](#)). [Kowalski et al. \(2009\)](#) attributed this result to a combination of increased flare visibility (the contrast between flare emission and the quiescent background emission of the star; [Gershberg 1972](#)) and an increase in the active fraction. They also proposed that later-type stars maintain their activity for longer: nearly 10 Gyr for M8 stars versus < 1 Gyr for M0 stars ([Shields et al. 2016](#); [West et al. 2006](#)).

In Figure 4 and Table 5, we show the distributions of ΔV and flare energies (see Section 3.1) broken down by spectral categories: M0–M1, M2–M3, and M4–M5. The M4–M5 group have the most flares among our sample, and they span a wider range of flare amplitudes than the M0–M1 and M2–M3 subgroups. Most of the M4–M5 flares have $0.25 \lesssim \Delta V \lesssim 0.5$ mag and jump to a $\Delta V \approx 2$ mag for I13352+3010, the largest amplitude confirmed flare.

All of the stars in the [Lépine et al. \(2013\)](#) sample have $H\alpha$ equivalent width (EW) measurements as a proxy for activity ([Walkowicz & Hawley 2009](#)). [Lépine et al. \(2013\)](#) and [West et al. \(2011\)](#) define active stars as those with $H\alpha$ EWs $< -0.75\text{\AA}$. The equivalent width of a line measures the strength of the spectral feature relative to the continuum, where the continuum varies with spectral type. Therefore, rather than using the EWs directly from [Lépine et al. \(2013\)](#), we use the χ ratio, defined as the ratio of the $H\alpha$ continuum to the bolometric luminosity ([West & Hawley 2008](#)). Multiplied by the $H\alpha$ EW, it gives the ratio of the $H\alpha$ luminosity to the bolometric luminosity, and it allows a direct comparison between the strengths of the $H\alpha$ features for stars of different spectral types.

We observe a strong correlation between activity and flaring: most of the stars with flares have negative χ values (see Figure 5). However, some stars with flares detected by ASAS-SN have low $H\alpha$ emission (the bottom row of Figure 2 shows flares of inactive stars). Of the 62 stars with flares, 55 stars are active ($\chi < 0$) and 7 are inactive ($\chi > 0$).

This result is consistent with other studies of M-dwarf flares. In particular, [Hilton et al. \(2011\)](#), [Kowalski et al. \(2009\)](#), and [Hawley et al. \(2014\)](#) studied populations of active and inactive M dwarfs and detected flares among both types, although they also found that active stars flare more frequently than inactive ones. [Newton et al. \(2017\)](#) showed that rapidly rotating stars (which tend to be younger with ages ≤ 2 Gyr: [Newton et al. 2016](#)) exhibit higher $H\alpha$ emission than slower rotators (which tend to be older, with ages ≥ 5 Gyr).

Finally, although we were not able to confirm flares on M dwarfs with spectral types later than M5, we note that a total of 40 stars between M5 and M9 were auto-

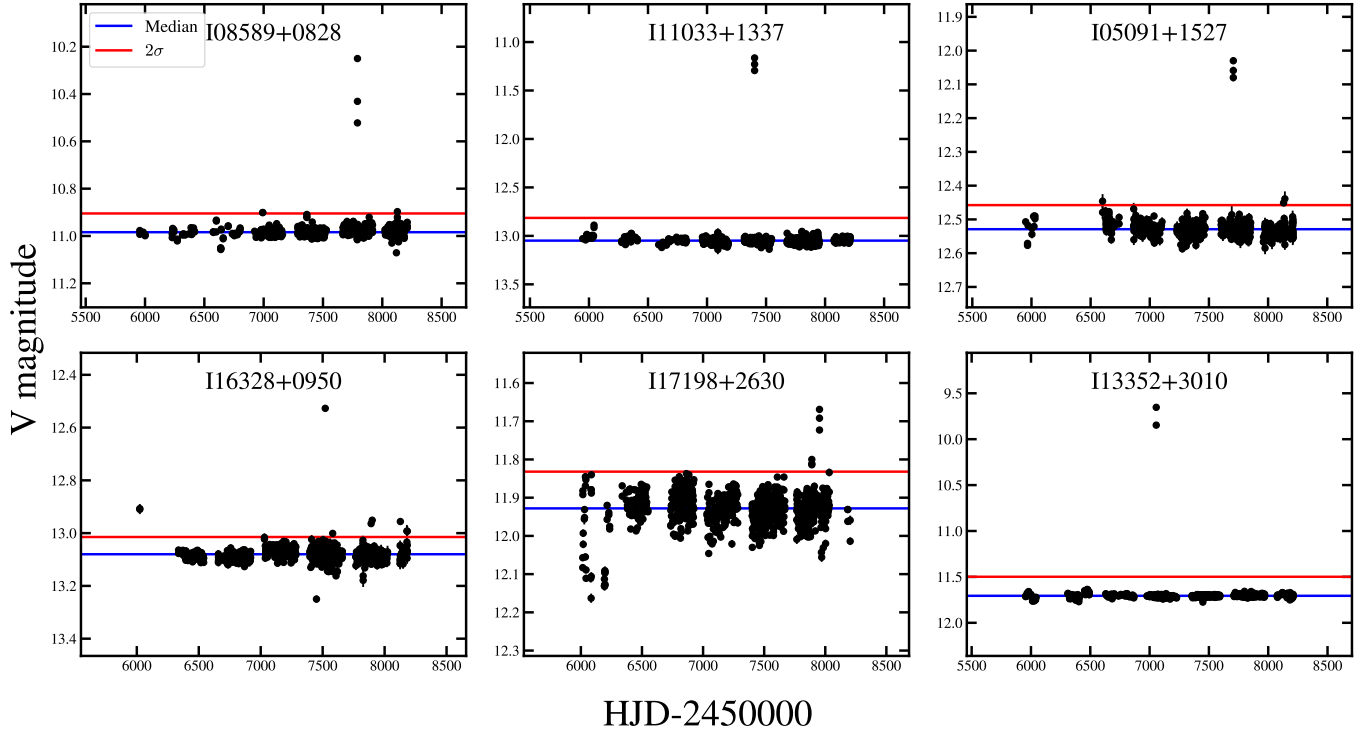


Figure 2. Representative examples of light curves from six of our flaring stars from the [Lépine et al. \(2013\)](#) sample. The red line shows the 2σ threshold for detection, while blue lines are the the mean magnitude. The top row consists of stars with $H\alpha$ in emission and the bottom row are stars with $H\alpha$ in absorption or weak.

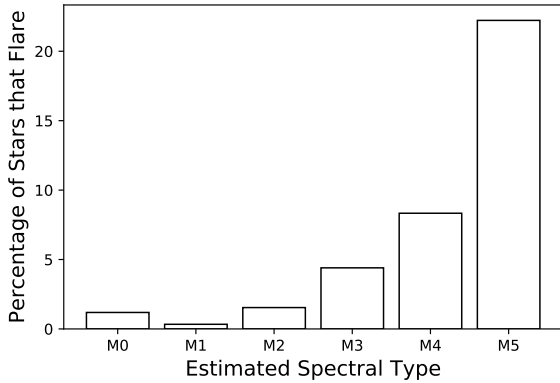


Figure 3. Distribution of spectral types among the final sample of flares from the [Lépine et al. \(2013\)](#) sample, representing $\sim 90\%$ of M dwarfs in the North. The histogram shows the number of stars from which we detected flares as a fraction of the total number of stars within each spectral class. The flaring fraction increases with spectral type, peaking at $\sim 25\%$ for the M5 class.

matically flagged by our algorithm in the [Lépine et al. \(2013\)](#) [18] and [Cruz et al. \(2007\)](#) [22] samples. It is likely that a fraction of those stars are truly flaring but did not meet our validation criteria. Despite the difficulty of characterizing flares on the lowest-mass stars,

studies have found them to be common (e.g. [Schmidt et al. 2014, 2016](#); [Gizis et al. 2017](#); [Vida et al. 2017](#); [Paudel et al. 2018, 2019](#)).

3.1. Flare energies

The relatively coarse sampling of our data gives little information about the morphology of individual flares, which is important for calculating flare energies (see Figure 6 in [Davenport et al. 2014](#) for an example of a 1-minute cadence light curve of a classical and complex flare). The energy of a flare is defined as the product of its equivalent duration (ED) and the quiescent luminosity of the star. The equivalent duration is the integrated area under the light curve and is measured in seconds ([Gershberg 1972](#)). We computed the quiescent luminosity of each star by multiplying the flux in the ASAS-SN bandpass by $4\pi d^2$, where d is the distance to the source as derived from [Bailer-Jones et al. \(2018\)](#), who uses the parallaxes from *Gaia* DR2 ([Gaia Collaboration et al. 2018](#)). For sources undetected by *Gaia*, we used the photometric parallaxes reported in [Lépine et al. \(2013\)](#). Although the limited cadence of our data prevents measurement of the ED of the flares directly, we can still place lower limits on the energies. We follow and briefly describe the methodology from [Schmidt et al. \(2018\)](#) to obtain flare EDs from a few detections.

Table 3. Stellar Properties

ID	Spt	ζ	$\log g$	T_{eff} (K)	Parallax ^a (mas)	Distance (pc)	H α EW (Å)
Confirmed Flares							
I00118+2259	M3.5	1.10	4.5	3260	48.860 ± 0.080	$20.45^{+0.03}_{-0.03}$	+0.30
I00162+1951W	M4.0	1.06	5.0	3250	4.290 ± 0.040	$15.18^{+0.02}_{-0.02}$	-4.01
I00325+0729	M4.0	1.05	4.5	3150	28.089 ± 0.155	$35.56^{+0.19}_{-0.19}$	-3.97
I01033+6221	M5.0	1.00	4.5	2940	101.637 ± 0.080	$9.83^{+0.007}_{-0.007}$	-8.06
I01593+5831	M4.0	1.04	5.0	3290	76.13 ± 0.054	$13.12^{+0.009}_{-0.009}$	-5.00
I02002+1303	M5.0	0.99	5.0	3130	223.634 ± 0.106	$4.47^{+0.002}_{-0.002}$	-0.83
I02088+4926	M4.0	0.93	5.0	3270	58.598 ± 0.078	$17.05^{+0.02}_{-0.02}$	-3.76
I02336+2455	M4.5	1.03	5.0	3130	0.579 ± 0.159	$9.96^{+0.01}_{-0.01}$	-3.06
I03394+2458	M3.5	0.97	5.0	3380	62.542 ± 0.079	$15.98^{+0.02}_{-0.02}$	-0.65
I04284+1741	M2.0	0.95	5.0	3590	21.817 ± 0.231	$46.83^{+0.58}_{-0.56}$	-1.95
I04480+1703	M0.5	0.92	4.5	3730	22.650 ± 0.451	$44.12^{+0.90}_{-0.86}$	+0.07
I05019+0108*	M4.5	1.00	5.0	3160	39.554 ± 0.083	$25.26^{+0.05}_{-0.05}$	-3.89
I05062+0439*	M4.0	1.01	4.5	3100	35.966 ± 0.054	$27.78^{+0.04}_{-0.04}$	-5.84
I05091+1527	M3.0	1.02	5.0	3520	33.617 ± 0.0730	$29.72^{+0.06}_{-0.06}$	-1.80
I05337+0156	M3.0	0.85	4.5	3350	63.598 ± 0.088	$15.71^{+0.02}_{-0.02}$	-4.98
I05547+1055*	M3.0	0.90	5.0	3530	40.520 ± 0.047	$24.66^{+0.02}_{-0.02}$	-3.55
I07364+0704	M5.0	0.96	4.5	2950	$149 \pm 44^{\dagger}$	6.71 ± 1.98	-3.55
I07384+2400 [†]	M3.5	0.89	5.0	3270	51.590 ± 0.058	$19.37^{+0.02}_{-0.02}$	-4.08
I07558+8323	M4.0	0.98	5.0	3250	76.352 ± 0.035	$13.09^{+0.006}_{-0.006}$	-3.27
I08589+0828	M4.5	0.95	5.0	3140	$215 \pm 63^{\dagger}$	4.65 ± 1.36	-2.74
I09177+4612	M2.5	0.92	4.5	3400	29.898 ± 0.424	$33.42^{+0.48}_{-0.47}$	-2.89
I10360+0507	M4.0	0.91	5.0	3140	65.381 ± 0.091	$15.28^{+0.02}_{-0.02}$	-2.80
I10367+1521*	M4.5	0.92	5.0	3100	50.621 ± 0.157	$19.74^{+0.06}_{-0.06}$	-4.46
I11033+1337	M4.0	0.90	5.0	3190	65.59 ± 0.09	$15.23^{+0.02}_{-0.02}$	-1.06
I12189+1107	M5.0	1.07	5.0	3110	154.507 ± 0.110	$6.47^{+0.004}_{-0.004}$	-3.53
I12332+0901	M5.5	1.00	4.5	2850	$258 \pm 76^{\dagger}$	3.87 ± 1.14	-4.51
I12485+4933*	M3.5	0.98	5.0	3370	40.771 ± 0.248	$24.51^{+0.15}_{-0.14}$	-4.73
I13007+1222	M1.5	0.91	4.5	3570	86.856 ± 0.151	$11.50^{+0.02}_{-0.02}$	-1.96
I13317+2916	M4.5	0.98	5.0	3150	54.687 ± 0.331	$18.27^{+0.11}_{-0.11}$	-7.51
I15126+4543	M4.0	1.01	5.0	3270	$64 \pm 19^{\dagger}$	15.62 ± 4.63	-3.19
I15218+2058	M2.0	0.95	4.5	3490	87.378 ± 0.049	$18.27^{+0.006}_{-0.006}$	-2.25
I15238+5609	M1.0	0.91	4.5	3570	19.657 ± 0.0260	$50.79^{+0.06}_{-0.06}$	-1.97
I15555+3512	M4.5	1.02	5.0	3130	35.942 ± 0.0440	$27.80^{+0.03}_{-0.03}$	-5.72
I15557+6840*	M2.5	0.98	5.0	3520	38.995 ± 0.024	$25.62^{+0.01}_{-0.01}$	-2.84
I15581+4927*	M1.0	0.86	4.5	3520	26.349 ± 0.021	$37.91^{+0.03}_{-0.03}$	-2.95
I16328+0950	M3.5	0.97	5.0	3270	65.047 ± 0.065	$15.36^{+0.01}_{-0.01}$	+0.31
I17198+2630	M3.5	1.02	4.5	3260	92.966 ± 0.061	$10.75^{+0.007}_{-0.007}$	-0.35
I17338+1655*	M5.5	1.02	5.0	2940	62.371 ± 0.390	$16.02^{+0.10}_{-0.10}$	-9.16
I18022+6415	M5.0	0.97	4.5	3040	$92 \pm 27^{\dagger}$	$7.78^{+0.003}_{-0.003}$	-3.17
I18358+8005	M4.0	0.95	5.0	3280	60.959 ± 0.041	$16.39^{+0.01}_{-0.01}$	-2.32
I18427+1354	M4.5	0.97	5.0	3100	91.429 ± 0.070	$10.93^{+0.008}_{-0.008}$	-2.26

^aTargets in bold are classified as Flare Stars or UV Ceti-type stars in Simbad or in VSX. Objects with a * are rotational variables. Parallax values with a [†] come from the photometric parallaxes reported in [Lépine et al. \(2013\)](#), while those without the [†] are from *Gaia* DR2. The ζ , $\zeta_{\text{TiO/CaH}}$ or “zeta” parameter is measured and defined in [Lépine et al. \(2013\)](#) as a combination of the TiO5, CaH2 and CaH3 spectral indices, a quantity shown to be correlated with metallicity in metal-poor, M subdwarfs and is $\zeta \simeq 1.05$ for solar abundances.

Table 3. Stellar Properties (continued)

ID	Spt	ζ	$\log g$	T_{eff} (K)	Parallax ^a (mas)	Distance (pc)	H α EW (\AA)
I19146+1919	M3.5	1.06	4.5	3300	3.491 ± 2.412	$18.09^{+0.02}_{-0.02}$	-3.29
I19539+4424E	M5.5	1.03	5.0	2930	$233 \pm 68^{\dagger}$	$4.66^{+0.001}_{-0.001}$	-2.57
I19539+4424W	M5.5	1.02	5.0	3030	$177 \pm 52^{\dagger}$	$4.69^{+0.01}_{-0.01}$	-2.00
I20198+2256*	M3.0	1.00	5.0	3400	34.080 ± 0.074	$29.31^{+0.06}_{-0.06}$	-3.27
I20298+0941	M5.0	0.96	4.5	2980	133.811 ± 1.386	$7.47^{+0.07}_{-0.07}$	-2.28
I20435+2407*	M2.5	0.91	5.0	3460	46.961 ± 0.045	$21.28^{+0.02}_{-0.02}$	-2.27
I21160+2951E*	M4.0	0.95	5.0	3260	49.214 ± 0.243	$20.30^{+0.10}_{-0.10}$	-3.78
I21376+0137	M4.5	1.01	5.0	3150	$75 \pm 22^{\dagger}$	13.33 ± 3.91	-9.40
I21521+0537	M3.5	0.96	5.0	3350	$58 \pm 17^{\dagger}$	17.24 ± 5.05	-3.97
I22012+2818	M4.5	0.95	5.0	3140	109.841 ± 0.059	$9.10^{+0.004}_{-0.004}$	-4.37
I22403+0754	M0.5	0.96	4.5	3640	24.240 ± 0.039	$41.20^{+0.06}_{-0.06}$	+0.33
I22468+4420	M4.0	0.98	5.0	3270	198.011 ± 0.038	$5.04^{+0.0009}_{-0.0009}$	-4.63
I22518+3145	M3.5	0.93	5.0	3400	$38 \pm 11^{\dagger}$	26.31 ± 7.61	-3.26
I23060+6355	M0.5	1.01	4.5	3650	41.539 ± 0.028	$24.05^{+0.01}_{-0.01}$	-1.44
I23548+3831*	M4.0	0.97	5.0	3250	59.346 ± 0.052	$16.84^{+0.01}_{-0.01}$	-3.74
I23578+3837*	M3.5	0.96	5.0	3380	47.305 ± 1.498	$21.16^{+0.69}_{-0.65}$	-3.47
I13352+3010	M0.0	1.02	4.5	3660	25.688 ± 0.057	$38.88^{+0.087}_{-0.086}$	+0.55
I16591+2058	M3.5	0.96	5.0	3370	56.182 ± 0.572	$17.79^{+0.18}_{-0.18}$	-2.18
I17006+0618	M1.0	0.94	4.5	3570	33.381 ± 0.040	$29.93^{+0.03}_{-0.03}$	+0.37
I20105+0632	M4.0	0.94	5.0	3270	62.367 ± 0.077	$16.02^{+0.02}_{-0.02}$	-4.39
I23340+0010	M2.5	1.08	5.0	3500	71.374 ± 0.049	$14.00^{+0.009}_{-0.009}$	+0.43
“Maybe” Flares							
I00570+4505	M3.0	0.98	5.0	3380	$57 \pm 17^{\dagger}$	17.54 ± 5.23	+0.45
I05342+1019N	M3.0	1.04	5.0	3400	45.17 ± 0.08	22.22 ± 0.039	+0.34
I07446+0333	M4.5	1.01	5.0	3130	167 ± 59	5.98 ± 0.002	-4.51
I09302+2630	M3.5	0.97	5.0	3290	41.15 ± 7	24.09 ± 0.04	-1.11
I12142+0037	M5.0	1.04	5.0	3040	$115 \pm 34^{\dagger}$	8.69 ± 2.57	-3.88
I12436+2506	M3.5	0.96	5.0	3280	43.65 ± 0.24	22.93 ± 5.76	-0.08
I13229+2428	M4.0	1.07	4.5	3130	$60 \pm 18^{\dagger}$	16.66 ± 5.0	+0.26
I19032+6359	M3.5	0.90	5.0	3380	$45 \pm 13^{\dagger}$	22.22 ± 6.41	-3.10

^aTargets in bold are classified as flare stars in Simbad. Parallax values with a † come from the photometric parallaxes reported in Lépine et al. (2013).

As in Schmidt et al. (2018), we fit our data by modifying the classical flare model from Davenport (2016). They characterized a flare using two free parameters: a scaled amplitude and the full-time width at half the maximum flux, denoted $t_{1/2}$. Their best-fit solution for the sharp rise is a fourth order polynomial of the form

$$F_{\text{rise}} = 1 + 1.941t_{1/2} - 0.175t_{1/2}^2 - 2.246t_{1/2}^3 - 1.125t_{1/2}^4 \quad (2)$$

while the decay, which contains 61% of the total energy, can be modeled as the sum of two exponentials:

$$F_{\text{decay}} = 0.6890 e^{-1.600t_{1/2}} + 0.3030 e^{-0.2783t_{1/2}} \quad (3)$$

We estimated the flare energies by generating 4000 flare light curves varying the position of the peak and $t_{1/2}$ ($10 < t_{1/2} < 2000$ seconds). We then integrated the flux of the flare compared to the stellar luminosity for each combination of peak position and $t_{1/2}$ and took the median of all the values as the estimate of the equivalent duration. After applying this procedure to our sample,

Table 4. Flare Properties

ID	Spt	Potential Flares	ΔV	E_V (erg)	E_U (erg)	E_{bol} (erg)	H α EW (Å)
I00118+2259	M3.5	3	0.22	$(1.99 \pm 0.95) \times 10^{32}$	$(3.59 \pm 1.72) \times 10^{32}$	$(4.72 \pm 2.26) \times 10^{33}$	+0.30
I00162+1951W	M4	1	0.16	$(2.28 \pm 0.75) \times 10^{34}$	$(4.11 \pm 1.35) \times 10^{34}$	$(5.41 \pm 1.78) \times 10^{35}$	-4.01
I00325+0729	M4	3	1.02	$(6.88 \pm 3.19) \times 10^{33}$	$(1.23 \pm 0.57) \times 10^{34}$	$(1.63 \pm 0.75) \times 10^{35}$	-3.97
I01033+6221	M5	3	0.24	$(5.92 \pm 2.60) \times 10^{31}$	$(1.06 \pm 0.46) \times 10^{32}$	$(1.40 \pm 0.61) \times 10^{33}$	-8.06
I01593+5831	M4	1	0.28	$(2.81 \pm 1.14) \times 10^{32}$	$(5.05 \pm 2.05) \times 10^{32}$	$(6.65 \pm 2.07) \times 10^{33}$	-5.00
I02002+1303	M5	2	0.87	$(2.67 \pm 0.26) \times 10^{31}$	$(4.82 \pm 0.47) \times 10^{31}$	$(6.34 \pm 0.62) \times 10^{32}$	-0.83
I02088+4926	M4	5	0.15	$(1.32 \pm 0.36) \times 10^{32}$	$(2.39 \pm 0.66) \times 10^{32}$	$(3.14 \pm 0.87) \times 10^{33}$	-3.76
I02336+2455	M4.5	6	0.20	$(6.88 \pm 1.10) \times 10^{35}$	$(1.23 \pm 0.19) \times 10^{36}$	$(1.63 \pm 0.26) \times 10^{37}$	-3.06
I03394+2458	M3.5	6	0.17	$(4.79 \pm 1.53) \times 10^{31}$	$(8.63 \pm 2.70) \times 10^{31}$	$(1.13 \pm 0.36) \times 10^{33}$	-0.65
I04284+1741	M2	2	0.12	$(1.26 \pm 0.57) \times 10^{33}$	$(2.26 \pm 1.04) \times 10^{33}$	$(2.98 \pm 1.37) \times 10^{34}$	-1.95
I04480+1703	M0.5	1	0.14	$(1.23 \pm 0.34) \times 10^{33}$	$(2.22 \pm 0.61) \times 10^{33}$	$(2.93 \pm 0.80) \times 10^{33}$	+0.07
I05019+0108	M4.5	7	0.20	$(4.06 \pm 1.24) \times 10^{32}$	$(7.31 \pm 2.23) \times 10^{32}$	$(9.62 \pm 2.94) \times 10^{33}$	-3.89
I05062+0439	M4	3	0.56	$(1.13 \pm 0.57) \times 10^{33}$	$(2.04 \pm 1.03) \times 10^{33}$	$(2.68 \pm 1.36) \times 10^{34}$	-5.89
I05091+1527	M3	2	0.50	$(2.12 \pm 0.93) \times 10^{33}$	$(3.82 \pm 1.68) \times 10^{33}$	$(5.03 \pm 2.22) \times 10^{34}$	-1.80
I05337+0156	M3	4	0.14	$(6.60 \pm 1.61) \times 10^{31}$	$(1.18 \pm 0.29) \times 10^{32}$	$(1.56 \pm 0.38) \times 10^{33}$	- 4.98
I05547+1055	M3	3	0.15	$(4.43 \pm 1.10) \times 10^{32}$	$(7.06 \pm 1.76) \times 10^{32}$	$(9.29 \pm 2.31) \times 10^{33}$	-3.55
I07364+0704	M5	3	0.60	$(1.51 \pm 0.32) \times 10^{31}$	$(2.72 \pm 0.58) \times 10^{31}$	$(3.58 \pm 0.76) \times 10^{32}$	-3.55
I07384+2400	M3.5	2	0.64	$(7.63 \pm 3.12) \times 10^{32}$	$(1.37 \pm 0.56) \times 10^{33}$	$(1.80 \pm 0.74) \times 10^{34}$	-4.08
I07558+8323	M4	7	0.19	$(6.27 \pm 2.95) \times 10^{31}$	$(1.12 \pm 0.53) \times 10^{32}$	$(1.48 \pm 0.69) \times 10^{33}$	-3.27
I08589+0828	M4.5	1	0.72	$(5.73 \pm 2.73) \times 10^{32}$	$(1.03 \pm 0.49) \times 10^{33}$	$(1.35 \pm 0.64) \times 10^{34}$	-2.74
I09177+4612	M2.5	4	0.23	$(1.00 \pm 0.48) \times 10^{33}$	$(1.80 \pm 0.86) \times 10^{33}$	$(2.37 \pm 1.13) \times 10^{34}$	-2.89
I10360+0507	M4.0	4	0.30	$(2.82 \pm 1.42) \times 10^{30}$	$(5.08 \pm 2.56) \times 10^{30}$	$(6.69 \pm 3.37) \times 10^{31}$	-2.80
I10367+1521	M4.5	2	0.80	$(4.45 \pm 2.00) \times 10^{32}$	$(8.02 \pm 3.60) \times 10^{32}$	$(1.05 \pm 0.47) \times 10^{34}$	-4.46
I11033+1337	M4	1	1.87	$(2.79 \pm 0.87) \times 10^{33}$	$(5.02 \pm 1.57) \times 10^{33}$	$(6.61 \pm 2.07) \times 10^{34}$	-1.06
I12189+1107	M5	5	0.28	$(1.08 \pm 0.42) \times 10^{31}$	$(1.96 \pm 0.76) \times 10^{31}$	$(2.58 \pm 1.00) \times 10^{32}$	-3.53
I12332+0901	M5.5	5	0.29	$(2.00 \pm 0.87) \times 10^{30}$	$(3.61 \pm 1.56) \times 10^{30}$	$(4.75 \pm 2.06) \times 10^{31}$	-4.51
I12485+4933	M3.5	5	0.23	$(3.94 \pm 1.87) \times 10^{32}$	$(7.09 \pm 3.37) \times 10^{32}$	$(9.34 \pm 4.43) \times 10^{33}$	-4.73
I13007+1222	M1.5	3	0.14	$(8.25 \pm 3.95) \times 10^{32}$	$(1.48 \pm 0.71) \times 10^{33}$	$(1.95 \pm 0.93) \times 10^{34}$	-1.96
I13317+2916	M4.5	7	0.20	$(2.97 \pm 1.42) \times 10^{32}$	$(5.35 \pm 2.57) \times 10^{32}$	$(7.04 \pm 3.82) \times 10^{33}$	-7.51
I15126+4543	M4	4	0.29	$(3.18 \pm 1.52) \times 10^{31}$	$(5.73 \pm 2.74) \times 10^{31}$	$(7.55 \pm 3.61) \times 10^{32}$	-3.19
I15218+2058	M2	1	0.17	$(6.47 \pm 3.10) \times 10^{32}$	$(1.16 \pm 0.55) \times 10^{33}$	$(1.53 \pm 0.73) \times 10^{34}$	-2.25
I15238+5609	M1	1	0.23	$(3.03 \pm 0.26) \times 10^{33}$	$(5.45 \pm 0.48) \times 10^{33}$	$(7.18 \pm 0.63) \times 10^{34}$	-1.97
I15555+3512	M4.5	4	0.33	$(1.07 \pm 0.47) \times 10^{31}$	$(1.93 \pm 0.86) \times 10^{31}$	$(2.55 \pm 1.13) \times 10^{32}$	-4.72
I15557+6840	M2.5	6	0.15	$(6.02 \pm 3.01) \times 10^{32}$	$(1.08 \pm 0.54) \times 10^{33}$	$(1.42 \pm 0.71) \times 10^{34}$	-2.84
I15581+4927	M1	7	0.51	$(2.14 \pm 0.41) \times 10^{33}$	$(3.86 \pm 0.07) \times 10^{33}$	$(5.08 \pm 0.09) \times 10^{34}$	-2.95
I16328+0950	M3.5	4	0.55	$(1.87 \pm 0.93) \times 10^{32}$	$(3.36 \pm 1.69) \times 10^{32}$	$(4.43 \pm 2.22) \times 10^{33}$	+0.31
I17198+2630	M3.5	2	0.26	$(2.07 \pm 0.98) \times 10^{32}$	$(3.73 \pm 1.77) \times 10^{32}$	$(4.91 \pm 2.33) \times 10^{33}$	-0.35
I17338+1655	M5.5	4	0.67	$(1.89 \pm 7.02) \times 10^{31}$	$(3.40 \pm 1.26) \times 10^{32}$	$(4.48 \pm 1.66) \times 10^{33}$	-9.16
I18022+6415	M5	4	0.73	$(4.74 \pm 1.60) \times 10^{31}$	$(8.53 \pm 2.88) \times 10^{31}$	$(1.12 \pm 0.37) \times 10^{33}$	-3.17
I18358+8005	M4	2	0.45	$(2.68 \pm 1.34) \times 10^{32}$	$(4.83 \pm 2.42) \times 10^{33}$	$(6.35 \pm 3.19) \times 10^{33}$	-2.32
I18427+1354	M4.5	4	0.60	$(4.92 \pm 1.24) \times 10^{31}$	$(8.86 \pm 2.23) \times 10^{31}$	$(1.16 \pm 0.29) \times 10^{33}$	-2.26
I19146+1919	M3.5	1	0.40	$(1.22 \pm 0.14) \times 10^{34}$	$(2.20 \pm 0.26) \times 10^{33}$	$(2.90 \pm 0.34) \times 10^{35}$	-3.29
I19539+4424E	M5.5	4	0.30	$(5.70 \pm 0.09) \times 10^{30}$	$(5.92 \pm 0.10) \times 10^{30}$	$(7.80 \pm 0.13) \times 10^{31}$	-2.57
I19539+4424W	M5.5	6	0.34	$(2.49 \pm 0.23) \times 10^{30}$	$(4.49 \pm 0.41) \times 10^{30}$	$(5.90 \pm 0.54) \times 10^{31}$	-2.00

NOTE—“Potential flares” is the number of events that pass the 2σ statistical cut, and ΔV is the magnitude of the largest flare observed. The potential flares are not necessarily confirmed; in some cases, only the largest flare was confirmed. E_U and E_{bol} are estimated from E_V using the relations from [Lacy et al. \(1976\)](#) and [Günther et al. \(2019\)](#).

Table 4. Flare Properties (continued)

ID	Spt	Potential Flares	ΔV	E_V (erg)	E_U (erg)	E_{bol} (erg)	H α EW (Å)
I20198+2256	M3	1	0.23	$(2.82 \pm 0.58) \times 10^{32}$	$(5.08 \pm 1.05) \times 10^{32}$	$(6.68 \pm 1.38) \times 10^{33}$	-3.27
I20298+0941	M5	4	0.78	$(7.32 \pm 3.61) \times 10^{31}$	$(1.31 \pm 0.64) \times 10^{32}$	$(1.73 \pm 0.85) \times 10^{33}$	-2.28
I20435+2407	M2.5	3	0.31	$(5.75 \pm 0.59) \times 10^{32}$	$(1.03 \pm 0.10) \times 10^{33}$	$(1.36 \pm 0.14) \times 10^{34}$	-2.27
I21160+2951E	M4	8	0.12	$(7.14 \pm 1.17) \times 10^{31}$	$(1.28 \pm 0.21) \times 10^{32}$	$(1.69 \pm 0.27) \times 10^{33}$	-3.78
I21376+0137	M4.5	8	0.12	$(1.55 \pm 0.60) \times 10^{33}$	$(2.94 \pm 1.15) \times 10^{33}$	$(3.87 \pm 1.52) \times 10^{34}$	-9.40
I21521+0537	M3.5	3	0.23	$(2.60 \pm 1.32) \times 10^{32}$	$(4.68 \pm 2.38) \times 10^{32}$	$(6.17 \pm 3.13) \times 10^{33}$	-3.97
I22012+2818	M4.5	2	0.73	$(1.19 \pm 0.41) \times 10^{32}$	$(2.14 \pm 0.74) \times 10^{32}$	$(2.82 \pm 0.98) \times 10^{33}$	-4.37
I22403+0754	M0.5	5	0.18	$(4.10 \pm 1.81) \times 10^{33}$	$(7.38 \pm 3.26) \times 10^{33}$	$(9.71 \pm 4.29) \times 10^{34}$	+0.33
I22468+4420	M4	5	0.18	$(3.48 \pm 1.10) \times 10^{31}$	$(6.26 \pm 1.98) \times 10^{31}$	$(8.24 \pm 2.61) \times 10^{32}$	-4.63
I22518+3145	M3.5	2	0.82	$(2.04 \pm 0.49) \times 10^{32}$	$(3.68 \pm 0.85) \times 10^{32}$	$(4.85 \pm 1.16) \times 10^{33}$	-3.26
I23060+6355	M0.5	2	0.19	$(2.23 \pm 0.44) \times 10^{33}$	$(3.68 \pm 0.88) \times 10^{32}$	$(5.29 \pm 1.05) \times 10^{33}$	-1.44
I23548+3831	M4	2	0.19	$(4.89 \pm 5.04) \times 10^{32}$	$(8.80 \pm 9.08) \times 10^{32}$	$(1.15 \pm 1.19) \times 10^{34}$	-3.74
I23578+3837	M3.5	5	0.26	$(2.09 \pm 0.60) \times 10^{32}$	$(3.77 \pm 1.09) \times 10^{32}$	$(4.96 \pm 1.43) \times 10^{33}$	-3.47
I13352+3010	M0	1	2.04	$(5.61 \pm 2.34) \times 10^{34}$	$(1.01 \pm 0.42) \times 10^{35}$	$(1.32 \pm 0.55) \times 10^{36}$	+0.55
I16591+2058	M3.5	1	1.11	$(5.34 \pm 0.91) \times 10^{32}$	$(3.97 \pm 0.68) \times 10^{32}$	$(5.23 \pm 0.90) \times 10^{33}$	-2.18
I17006+0618	M1	1	0.45	$(2.43 \pm 1.23) \times 10^{33}$	$(4.37 \pm 2.22) \times 10^{33}$	$(5.75 \pm 2.93) \times 10^{34}$	+0.37
I20105+0632	M4	4	0.12	$(4.62 \pm 1.50) \times 10^{31}$	$(8.31 \pm 2.70) \times 10^{31}$	$(1.09 \pm 3.55) \times 10^{32}$	-4.39
I23340+0010	M2.5	3	0.27	$(3.94 \pm 1.09) \times 10^{32}$	$(7.09 \pm 1.96) \times 10^{32}$	$(9.33 \pm 2.59) \times 10^{33}$	+0.43

Table 5. Flaring Statistics by Spectral Type

Spt	# Stars	Median ΔV (mag)	Median E_V (erg)
M0–M1	9	0.19	2.2×10^{33}
M2–M3	21	0.23	3.9×10^{32}
M4–M5	32	0.30	7.2×10^{31}

we derived energies ranging from $2.0 \times 10^{30} < E_V < 6.9 \times 10^{35}$ ergs. The energies are listed in Table 4, and we plot the flare energies as a function of spectral type in Figure 5.

To estimate the bolometric energy E_{bol} of the flare from the V -band energy E_V , we used the conversions from Lacy et al. (1976) and in Günther et al. (2019). Lacy et al. (1976) determined flare energy scaling relations based on simultaneous, multi-wavelength observations of flares in the U , B and V filters. They found that the U , B and V energies scale as $E_U = 1.2E_B$ and $E_U = 1.8E_V$. Based on M dwarfs observed with *TESS*, Günther et al. (2019) convert their derived bolometric flare energies to U -band energies as $E_U \approx 0.076E_{\text{bol}}$. Combining these relations, we find that $E_V \approx 0.042E_{\text{bol}}$, and we list the resulting E_{bol} in Table 4.

3.2. Variability Analysis

To explore the connection between magnetic activity and stellar rotation, we estimated rotational periods for the stars in the Lépine et al. (2013) sample from the ASAS-SN light curves. We did not consider the Cruz et al. 2007 sample here because of the stars' faintness. We used the *astropy* implementation of the Generalized Lomb-Scargle (GLS; Zechmeister & Kürster 2009; Scargle 1982) periodogram and the *astrobase* implementation (Bhatti et al. 2018) of the Box Least Squares (BLS; Kovács et al. 2002) periodogram to search for periodicity over the range $0.05 \leq P \leq 100$ days. Periodic sources were classified using a random forest classifier and quality checks as described in Jayasinghe et al. (2019). In order to minimize false positives due to spurious variability signals in the data, we implemented cuts in classification probability $\text{Prob} > 0.9$ and the Lafler-Kinmann string length statistic (Lafler & Kinman 1965; Clarke 2002; Jayasinghe et al. 2019) calculated for the magnitudes sorted by phase $T(\phi|P) < 0.65$.

Among the 1276 dwarfs in the Lépine et al. (2013) sample, we identified 77 rotational variables (see Table 6) and 40 other variables (see Table 7). The source I16343+5709 had $\text{Prob} = 0.80$, but upon visual verification, we found that it was the known detached eclipsing

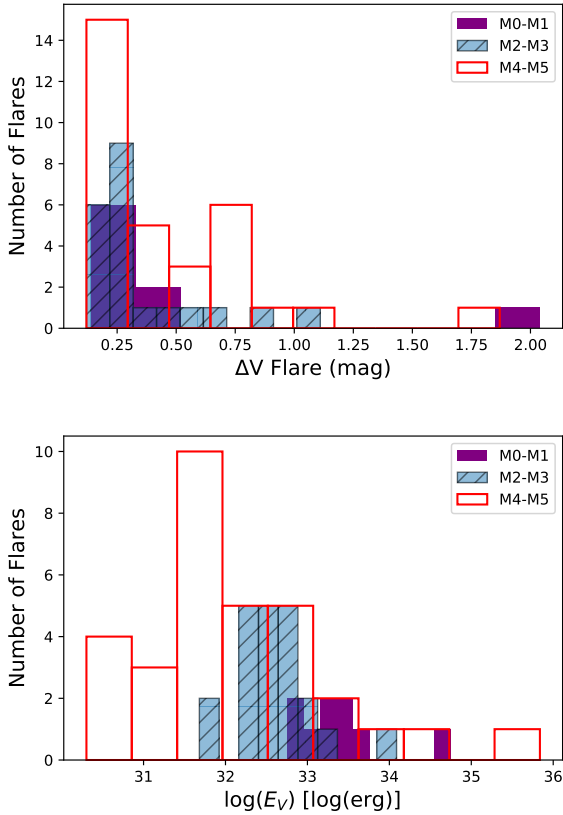


Figure 4. Distribution of ΔV mag (**top**) and V-band energies E_V (**bottom**) for the sample of validated flares divided into 3 spectral type groups: M0–M1, M2–M3, and M4–M5 stars.

binary CM Draconis with $P = 1.2684$ days (Morales et al. 2009).

14 rotational variables had flares identified in the ASAS-SN data, which amounts to $\sim 23\%$ of the flaring sample. 13 of those have rotation periods between $1.1 < P < 14.2$ days (and an additional one has $P = 97.1$ d) and a median value of $P = 3.8$ days. They have $H\alpha$ EWs of $< -2\text{\AA}$ and a median EW of -3.7\AA . On the other hand, the rotational variables with no confirmed flares have weaker $H\alpha$ emission, with EWs of -4.4\AA to $+0.62\text{\AA}$ and a median value of -0.24\AA . Thus, the rotational variables with identified flares are more active than those without detected flares. In agreement with previous studies (e.g., Newton et al. 2017; Doyle et al. 2018), we find that more “active” stars (which exhibit starspot modulations and flares) have rotation periods of $\lesssim 10$ days, while the more inactive stars (as defined by weaker $H\alpha$ emission and lack of detectable flares) have longer rotation periods. There are exceptions to this trend, such as the active, flaring star I20198+2256 (which has $P \sim 97$ days) or the active M5.5 star Proxima

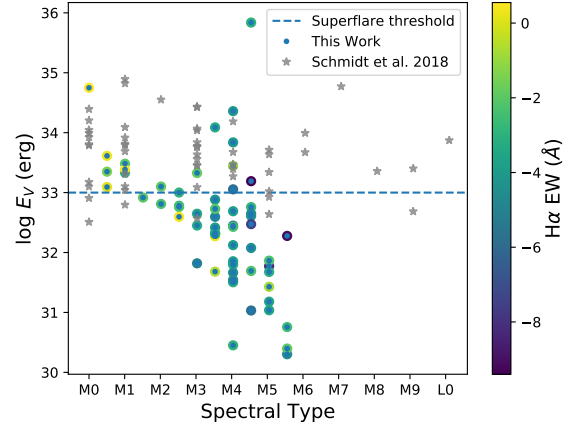


Figure 5. Energy in V-band (E_V) of the largest confirmed flare for each star by spectral subtype. The “superflare” threshold marked by the horizontal dashed line denotes flares with V-band energies $\gtrsim 10^{33}$ erg. The colors on the data points represent the values of the χ ratio, which is proportional to the ratio of the $H\alpha$ luminosity to the bolometric luminosity of a star.

Centaury (which has $P \sim 83$ days), both slow rotators compared to other stars with comparable flare rates and activity levels (Davenport 2016).

3.3. Influence on exoplanets

To find how many stars in our sample host confirmed exoplanets, we cross-matched our targets to the NASA Exoplanet Archive¹ by coordinate and checked for planets found by any method. In the flaring sample, we found 1 confirmed exoplanet around I13007+1222 ($\Delta V = 0.14$, Spt = M1.5V) and one star with a threshold-crossing event (TCE), I19539+4424W, where a TCE is a series of transit-like features resembling a true exoplanet signature (Jenkins et al. 2002). However, this star is in a binary with I19539+4424E, and therefore the TCE could be due to the stars eclipsing one another rather than a real planet.

In the full Lépine et al. (2013) sample, we found 6 confirmed planets (1 per star) associated with I04520+0628, I08551+0132, I11421+2642, I13007+1222, I16167+6714, and I16581+2544. Of those, I04520+0628 and I11421+2642 were identified as potential candidates by our flare-finding algorithm. We confirmed at least one flare around I13007+1222 with an energy of $(8.25 \pm 3.95) \times 10^{32}$ erg.

Flares can have adverse effects on the habitability of M-dwarf planets. Long-term, frequent exposure to

¹ <https://exoplanetarchive.ipac.caltech.edu/>

Table 6. Rotational Variable Stars

ID	Probability	Period (days)	ID	Probability	Period (days)
I00505+2449S	0.991	9.656	I09275+5039	0.978	18.93
I00081+4757	0.963	8.751	I09352+6114	0.917	97.32
I00084+1725	0.979	15.363	I10043+5023	0.975	3.067
I00268+7008	0.974	18.195	I10367+1521*	0.946	7.153
I01036+4051	0.998	28.445	I11118+3332S	0.968	15.54
I01066+1516	0.973	35.010	I11519+0731	0.995	6.878
I02028+0447	0.995	15.869	I12156+5239	0.965	4.891
I02180+5616	0.982	1.782	I12485+4933*	0.993	4.063
I02292+1932	0.999	5.546	I13518+1247	0.957	4.967
I03168+8205	0.976	16.640	I14023+1341	0.974	1.496
I03247+4447	0.972	2.053	I14153+1523	0.986	23.93
I03322+4914S	0.999	5.947	I15280+2547	0.984	26.17
I03466+8207	0.977	1.248	I15557+6840*	0.994	3.920
I04274+2022	0.982	43.61	I15581+4927*	0.977	4.492
I04312+4217	0.999	3.960	I15597+4403	0.991	1.480
I04350+0839	0.999	11.75	I16046+2620	0.973	16.80
I04473+0627	0.987	87.25	I16139+3346	0.982	24.59
I04595+0147	0.999	4.384	I16220+2250	0.994	5.489
I00483+7116	0.990	9.488	I17225+0531	0.964	67.65
I05019+0108*	0.991	4.187	I17338+1655*	0.919	1.325
I05062+0439*	0.962	2.666	I18134+0526	0.944	0.793
I05228+2016	0.938	28.93	I18312+0650	0.940	1.046
I05334+4809	0.977	14.27	I18519+1300	0.994	5.971
I05341+4732	0.999	12.428	I18554+0824	0.992	12.58
I05365+1119	0.988	2.018	I19026+3231	0.995	3.545
I05402+1239	0.960	6.331	I19270+1242	0.986	3.478
I05547+1055*	0.987	1.130	I19354+3746	0.994	8.258
I06025+3707	0.975	31.53	I20198+2256*	0.944	97.16
I06147+4727	0.977	27.20	I20220+2147	0.974	38.20
I06212+4414	0.991	5.728	I20435+2407*	0.987	2.398
I06237+0502	0.967	71.35	I21152+2547	0.988	48.60
I06262+2349	0.967	15.77	I21160+2951E*	0.985	1.759
I06310+5002	0.995	15.25	I22006+2715	0.999	10.59
I07295+3556	0.989	2.673	I22107+0754	0.980	14.91
I07346+2220	0.980	27.94	I22129+5504N	0.966	4.834
I07349+1445	0.982	20.08	I23318+1956E	0.958	15.28
I07384+2400*	0.972	3.857	I23548+3831*	0.965	14.29
I08317+0545	0.979	1.786	I23578+3837*	0.952	2.665
I09161+0153	0.972	4.308			

NOTE—Objects with a * are those identified to have flares in the ASAS-SN data.

Table 7. Other Variable Stars

ID	Probability	Period (days)	ID	Probability	Period (days)
I00173+2910	0.967	39.45	I13293+1126	0.927	57.13
I01025+7140	0.924	50.90	I15043+6023	0.951	38.43
I01453+4632	0.964	4.093	I17198+4142	0.952	62.24
I01593+5831	0.961	4.144	I18319+4041	0.966	45.47
I02070+4938	0.978	28.00	I20151+6331	0.976	28.94
I02088+4926	0.965	1.496	I20450+4429	0.931	75.75
I02116+1833	0.946	61.93	I21013+3314	0.965	2.960
I03479+0247	0.965	3.990	I21402+3703	0.983	2.990
I04520+0628	0.908	50.66	I21442+0638	0.987	62.68
I05333+4448	0.958	42.16	I21448+4417	0.923	78.61
I06579+6219	0.918	53.88	I21521+0537	0.985	0.938
I07446+0333	0.951	11.11	I22234+3227	0.985	5.937
I08095+2154	0.971	25.46	I22468+4420	0.943	4.362
I08371+1507	0.940	53.74	I22518+3145	0.950	4.922
I09187+2645	0.970	26.96	I23045+6645	0.954	26.39
I09193+6203	0.919	2.922	I23182+4617	0.962	17.38
I09428+7002	0.969	24.10	I23216+1717	0.936	78.22
I10360+0507	0.929	6.843	I23293+4128	0.963	4.252
I11237+0833	0.969	39.69	I23318+1956Wn	0.957	2.134
I12428+4153	0.942	66.67	I23431+3632	0.934	71.73

flares, coronal mass ejections, stellar proton events, and other related phenomena can cause atmospheric erosion over time (Lammer et al. 2007; Segura et al. 2010; Luger & Barnes 2015; Tilley et al. 2017; Howard et al. 2018, 2019; Loyd et al. 2018). For example, Tilley et al. (2017) modeled the impact of M-dwarf flares on an Earth-like, unmagnetized exoplanet in the habitable zone of its host star. They found that flares with energies comparable to 10^{34} erg in the U -band with a frequency $\gtrsim 1$ per month will erode $\sim 99\%$ of the ozone layer. Converting V -band to U -band energies using $E_U = 1.8E_V$, we find 5 sources with flare energies $\gtrsim 10^{34}$ erg. We did not construct a flare frequency distribution (FFD) because we only confirmed the largest flare in each star, and therefore we do not constrain the frequency of flares at this energy. However, we estimate that such high-energy events are relatively infrequent: in stars where we confirm a large flare, we do not find other flares of comparable amplitude (or energy) in the 6-year light curves. Flare distributions are power laws (Hawley et al. 2014), and high-energy flares are less common than low-energy ones. We do see frequent, small flare-like features (some are apparent in the light curves in Figure 2), and it is possible that even small, low-energy events like microflares ($E_V \sim 10^{29}$ erg) that occur sufficiently frequently could cause irreversible

damage to an Earth-like atmosphere and complex surface life (e.g., Günther et al. 2019).

4. CONCLUSIONS

In this paper, we performed an optical search for stellar flares of ~ 1400 M dwarfs using long-baseline, moderate-cadence photometry from ASAS-SN. The sample was comprised of the brightest ($J < 9$ mag) M dwarfs in the northern hemisphere and the nearest ($d < 20$ pc) M dwarfs. Applying a simple flare-finding algorithm, we automatically detected 480 stars with potential flares, of which 62 were confirmed after visual inspection of the data. The confirmed events range in amplitude of $0.12 < \Delta V < 2.04$ mag and have V -band energies of $2.0 \times 10^{30} \lesssim E_V \lesssim 6.9 \times 10^{35}$ erg, consistent with previous results in the literature.

From our sample of confirmed flares, we find a strong trend in the flaring fraction as a function of spectral type: the cooler M dwarfs flare more, with 25% of all M5 dwarfs in our sample flaring. We were not able to confirm flares among the later-types (from M6–M9) because the majority of the coolest dwarfs are optically faint and are therefore near or beyond the detection limits of the instruments. We find a positive correlation between the $H\alpha$ equivalent width and the flaring fraction: stars in our confirmed flare sample display strong $H\alpha$

emission. Finally, we derive rotation periods for stars in the [Lépine et al. \(2013\)](#) sample and find that the rotational variables with detected flares have stronger H α emission and relatively shorter periods than those without detected flares.

Flares and stellar activity impact the habitability of exoplanets around M dwarfs. Observations at higher cadence and across wavebands, such as with *TESS* and *JWST*, are crucial to measure flaring frequency and reliable flare bolometric energies. Overall, these constraints are crucial to probe the relationship between flares, magnetic fields, rotation, and stellar age.

We thank Dr. Jennifer van Saders and Dr. Kris Stanek for useful discussions that enriched this project. B.J.S. is supported by NSF grant AST-1908952. ASAS-SN is supported by the Gordon and Betty Moore Foundation through grant GBMF5490 to the Ohio State University and NSF grant AST-1515927. Development of ASAS-SN has been supported by NSF grant AST-0908816, the Mt. Cuba Astronomical Foundation, the Center for Cosmology and AstroParticle Physics at the Ohio State University, the Chinese Academy of Sciences South America Center for Astronomy (CASSACA), the Villum Foundation, and George Skestos.

REFERENCES

- Allard, F., Homeier, D., & Freytag, B. 2011, in *Astronomical Society of the Pacific Conference Series*, Vol. 448, 16th Cambridge Workshop on Cool Stars, Stellar Systems, and the Sun, ed. C. Johns-Krull, M. K. Browning, & A. A. West, 91
- Bailer-Jones, C. A. L., Rybizki, J., Foesneau, M., Mantelet, G., & Andrae, R. 2018, *AJ*, 156, 58, doi: [10.3847/1538-3881/aac21](#)
- Bhatti, W., Igbouma, Joshua, & Price-Whelan, A. 2018, *Waqasbhatti/Astrobase: Astrobase V0.3.14, v0.3.14*, Zenodo, doi: [10.5281/zenodo.1246769](#)
- Bochanski, J. J., Hawley, S. L., Covey, K. R., et al. 2010, *AJ*, 139, 2679, doi: [10.1088/0004-6256/139/6/2679](#)
- Borucki, W. J., Koch, D., Basri, G., et al. 2010, *Science*, 327, 977, doi: [10.1126/science.1185402](#)
- Carrington, R. C. 1859, *MNRAS*, 20, 13, doi: [10.1093/mnras/20.1.13](#)
- Chabrier, G., & Baraffe, I. 1997, *A&A*, 327, 1039
- Clarke, D. 2002, *A&A*, 386, 763, doi: [10.1051/0004-6361:20020258](#)
- Cruz, K. L., Reid, I. N., Kirkpatrick, J. D., et al. 2007, *AJ*, 133, 439, doi: [10.1086/510132](#)
- Davenport, J. R. A. 2016, *ApJ*, 829, 23, doi: [10.3847/0004-637X/829/1/23](#)
- Davenport, J. R. A., Becker, A. C., Kowalski, A. F., et al. 2012, *ApJ*, 748, 58, doi: [10.1088/0004-637X/748/1/58](#)
- Davenport, J. R. A., Hawley, S. L., Hebb, L., et al. 2014, *ApJ*, 797, 122, doi: [10.1088/0004-637X/797/2/122](#)
- Doyle, L., Ramsay, G., Doyle, J. G., Wu, K., & Scullion, E. 2018, *MNRAS*, 480, 2153, doi: [10.1093/mnras/sty1963](#)
- Dressing, C. D., & Charbonneau, D. 2015, *ApJ*, 807, 45, doi: [10.1088/0004-637X/807/1/45](#)
- France, K., Froning, C. S., Linsky, J. L., et al. 2013, *ApJ*, 763, 149, doi: [10.1088/0004-637X/763/2/149](#)
- Gaia Collaboration, Brown, A. G. A., Vallenari, A., et al. 2018, *A&A*, 616, A1, doi: [10.1051/0004-6361/201833051](#)
- Gershberg, R. E. 1972, *Ap&SS*, 19, 75, doi: [10.1007/BF00643168](#)
- . 2005, *Solar-Type Activity in Main-Sequence Stars*, doi: [10.1007/3-540-28243-2](#)
- Gizis, J. E., Monet, D. G., Reid, I. N., et al. 2000, *AJ*, 120, 1085, doi: [10.1086/301456](#)
- Gizis, J. E., Paudel, R. R., Schmidt, S. J., Williams, P. K. G., & Burgasser, A. J. 2017, *ApJ*, 838, 22, doi: [10.3847/1538-4357/aa6197](#)
- Günther, M. N., Zhan, Z., Seager, S., et al. 2019, *arXiv e-prints*, arXiv:1901.00443, <https://arxiv.org/abs/1901.00443>
- Hawley, S. L., Davenport, J. R. A., Kowalski, A. F., et al. 2014, *ApJ*, 797, 121, doi: [10.1088/0004-637X/797/2/121](#)
- Hawley, S. L., Gizis, J. E., & Reid, I. N. 1996, *AJ*, 112, 2799, doi: [10.1086/118222](#)
- Hilton, E. J., Hawley, S. L., Kowalski, A. F., & Holtzman, J. 2011, in *Astronomical Society of the Pacific Conference Series*, Vol. 448, 16th Cambridge Workshop on Cool Stars, Stellar Systems, and the Sun, ed. C. Johns-Krull, M. K. Browning, & A. A. West, 197
- Howard, W. S., Corbett, H., Law, N. M., et al. 2019, *ApJ*, 881, 9, doi: [10.3847/1538-4357/ab2767](#)
- Howard, W. S., Tilley, M. A., Corbett, H., et al. 2018, *ApJL*, 860, L30, doi: [10.3847/2041-8213/aacaf3](#)
- Ilin, E., Schmidt, S. J., Davenport, J. R. A., & Strassmeier, K. G. 2018, in *20th Cambridge Workshop on Cool Stars, Stellar Systems and the Sun*, 1
- Jayasinghe, T., Kochanek, C. S., Stanek, K. Z., et al. 2018, *MNRAS*, 477, 3145, doi: [10.1093/mnras/sty838](#)
- Jayasinghe, T., Stanek, K. Z., Kochanek, C. S., et al. 2019, *MNRAS*, 486, 1907, doi: [10.1093/mnras/stz844](#)
- Jenkins, J. M., Caldwell, D. A., & Borucki, W. J. 2002, *ApJ*, 564, 495, doi: [10.1086/324143](#)
- Jones, D. O., & West, A. A. 2016, *ApJ*, 817, 1, doi: [10.3847/0004-637X/817/1/1](#)

- Kaiser, N. 2004, in *Proc. SPIE*, Vol. 5489, Ground-based Telescopes, ed. J. M. Oschmann, Jr., 11–22
- Kiraga, M., & Stepien, K. 2007, *AcA*, 57, 149.
<https://arxiv.org/abs/0707.2577>
- Kochanek, C. S., Shappee, B. J., Stanek, K. Z., et al. 2017, *PASP*, 129, 104502, doi: [10.1088/1538-3873/aa80d9](https://doi.org/10.1088/1538-3873/aa80d9)
- Kovács, G., Zucker, S., & Mazeh, T. 2002, *A&A*, 391, 369, doi: [10.1051/0004-6361:20020802](https://doi.org/10.1051/0004-6361:20020802)
- Kowalski, A. F., Hawley, S. L., Hilton, E. J., et al. 2009, *AJ*, 138, 633, doi: [10.1088/0004-6256/138/2/633](https://doi.org/10.1088/0004-6256/138/2/633)
- Kowalski, A. F., Hawley, S. L., Holtzman, J. A., Wisniewski, J. P., & Hilton, E. J. 2010, *ApJL*, 714, L98, doi: [10.1088/2041-8205/714/1/L98](https://doi.org/10.1088/2041-8205/714/1/L98)
- Kowalski, A. F., Hawley, S. L., Wisniewski, J. P., et al. 2013, *ApJS*, 207, 15, doi: [10.1088/0067-0049/207/1/15](https://doi.org/10.1088/0067-0049/207/1/15)
- Lacy, C. H., Moffett, T. J., & Evans, D. S. 1976, *ApJS*, 30, 85, doi: [10.1086/190358](https://doi.org/10.1086/190358)
- Lafler, J., & Kinman, T. D. 1965, *ApJS*, 11, 216, doi: [10.1086/190116](https://doi.org/10.1086/190116)
- Lammer, H., Lichtenegger, H. I. M., Kulikov, Y. N., et al. 2007, *Astrobiology*, 7, 185, doi: [10.1089/ast.2006.0128](https://doi.org/10.1089/ast.2006.0128)
- Law, N. M., Kulkarni, S. R., Dekany, R. G., et al. 2009, *PASP*, 121, 1395, doi: [10.1086/648598](https://doi.org/10.1086/648598)
- Lépine, S., Hilton, E. J., Mann, A. W., et al. 2013, *AJ*, 145, 102, doi: [10.1088/0004-6256/145/4/102](https://doi.org/10.1088/0004-6256/145/4/102)
- Lloyd, R. O. P., France, K., Youngblood, A., et al. 2018, *ApJ*, 867, 71, doi: [10.3847/1538-4357/aae2bd](https://doi.org/10.3847/1538-4357/aae2bd)
- Luger, R., & Barnes, R. 2015, *Astrobiology*, 15, 119, doi: [10.1089/ast.2014.1231](https://doi.org/10.1089/ast.2014.1231)
- Mondrik, N., Newton, E., & Irwin, D. C. J. 2018, *ArXiv e-prints*. <https://arxiv.org/abs/1809.09177>
- Morales, J. C., Ribas, I., Jordi, C., et al. 2009, *ApJ*, 691, 1400, doi: [10.1088/0004-637X/691/2/1400](https://doi.org/10.1088/0004-637X/691/2/1400)
- Newton, E. R., Irwin, J., Charbonneau, D., et al. 2017, *ApJ*, 834, 85, doi: [10.3847/1538-4357/834/1/85](https://doi.org/10.3847/1538-4357/834/1/85)
- . 2016, *ApJ*, 821, 93, doi: [10.3847/0004-637X/821/2/93](https://doi.org/10.3847/0004-637X/821/2/93)
- O’Malley-James, J. T., & Kaltenegger, L. 2019, *MNRAS*, 485, 5598, doi: [10.1093/mnras/stz724](https://doi.org/10.1093/mnras/stz724)
- Paudel, R. R., Gizis, J. E., Mullan, D. J., et al. 2018, *ApJ*, 858, 55, doi: [10.3847/1538-4357/aab8fe](https://doi.org/10.3847/1538-4357/aab8fe)
- . 2019, *MNRAS*, 486, 1438, doi: [10.1093/mnras/stz886](https://doi.org/10.1093/mnras/stz886)
- Pojmanski, G. 1997, *AcA*, 47, 467
- Poppenhaeger, K. 2015, in *European Physical Journal Web of Conferences*, Vol. 101, European Physical Journal Web of Conferences, 05002
- Ricker, G. R., Winn, J. N., Vanderspek, R., et al. 2015, *Journal of Astronomical Telescopes, Instruments, and Systems*, 1, 014003, doi: [10.1117/1.JATIS.1.1.014003](https://doi.org/10.1117/1.JATIS.1.1.014003)
- Rodríguez, R., Schmidt, S. J., Jayasinghe, T., et al. 2018, *Research Notes of the American Astronomical Society*, 2, 8, doi: [10.3847/2515-5172/aabe7d](https://doi.org/10.3847/2515-5172/aabe7d)
- Samus’, N. N., Goranskii, V. P., Durlevich, O. V., et al. 2003, *Astronomy Letters*, 29, 468, doi: [10.1134/1.1589864](https://doi.org/10.1134/1.1589864)
- Scargle, J. D. 1982, *ApJ*, 263, 835, doi: [10.1086/160554](https://doi.org/10.1086/160554)
- Schmidt, S. J., Prieto, J. L., Stanek, K. Z., et al. 2014, *ApJL*, 781, L24, doi: [10.1088/2041-8205/781/2/L24](https://doi.org/10.1088/2041-8205/781/2/L24)
- Schmidt, S. J., Shappee, B. J., Gagné, J., et al. 2016, *ApJL*, 828, L22, doi: [10.3847/2041-8205/828/2/L22](https://doi.org/10.3847/2041-8205/828/2/L22)
- Schmidt, S. J., Shappee, B. J., van Saders, J. L., et al. 2018, *ArXiv e-prints*. <https://arxiv.org/abs/1809.04510>
- Segura, A., Walkowicz, L. M., Meadows, V., Kasting, J., & Hawley, S. 2010, *Astrobiology*, 10, 751, doi: [10.1089/ast.2009.0376](https://doi.org/10.1089/ast.2009.0376)
- Shappee, B. J., Prieto, J. L., Grupe, D., et al. 2014, *ApJ*, 788, 48, doi: [10.1088/0004-637X/788/1/48](https://doi.org/10.1088/0004-637X/788/1/48)
- Shields, A. L., Ballard, S., & Johnson, J. A. 2016, *PhR*, 663, 1, doi: [10.1016/j.physrep.2016.10.003](https://doi.org/10.1016/j.physrep.2016.10.003)
- Simonian, G., Stanek, K. Z., Schmidt, S., et al. 2016, *The Astronomer’s Telegram*, 8803
- Stanek, K. Z., Shappee, B. J., Kochanek, C. S., et al. 2013, *The Astronomer’s Telegram*, 5276
- Tilley, M. A., Segura, A., Meadows, V. S., Hawley, S., & Davenport, J. 2017, *arXiv e-prints*, arXiv:1711.08484. <https://arxiv.org/abs/1711.08484>
- Tyson, J. A. 2002, in *Proc. SPIE*, Vol. 4836, Survey and Other Telescope Technologies and Discoveries, ed. J. A. Tyson & S. Wolff, 10–20
- Vida, K., Kővári, Z., Pál, A., Oláh, K., & Kriskovics, L. 2017, *ApJ*, 841, 124, doi: [10.3847/1538-4357/aa6f05](https://doi.org/10.3847/1538-4357/aa6f05)
- Vida, K., Kriskovics, L., & Oláh, K. 2013, *Astronomische Nachrichten*, 334, 972, doi: [10.1002/asna.201211973](https://doi.org/10.1002/asna.201211973)
- Vida, K., Oláh, K., & Szabó, R. 2014, *MNRAS*, 441, 2744, doi: [10.1093/mnras/stu760](https://doi.org/10.1093/mnras/stu760)
- Walkowicz, L. M., & Hawley, S. L. 2009, *AJ*, 137, 3297, doi: [10.1088/0004-6256/137/2/3297](https://doi.org/10.1088/0004-6256/137/2/3297)
- Watson, C. L., Henden, A. A., & Price, A. 2006, *Society for Astronomical Sciences Annual Symposium*, 25, 47
- Wenger, M., Ochsenbein, F., Egret, D., et al. 2000, *A&AS*, 143, 9, doi: [10.1051/aas:2000332](https://doi.org/10.1051/aas:2000332)
- West, A. A., Bochanski, J. J., Hawley, S. L., et al. 2006, *AJ*, 132, 2507, doi: [10.1086/508652](https://doi.org/10.1086/508652)
- West, A. A., & Hawley, S. L. 2008, *PASP*, 120, 1161, doi: [10.1086/593024](https://doi.org/10.1086/593024)
- West, A. A., Hawley, S. L., Bochanski, J. J., et al. 2008, *AJ*, 135, 785, doi: [10.1088/0004-6256/135/3/785](https://doi.org/10.1088/0004-6256/135/3/785)
- West, A. A., Hawley, S. L., Walkowicz, L. M., et al. 2004, *AJ*, 128, 426, doi: [10.1086/421364](https://doi.org/10.1086/421364)

- West, A. A., Morgan, D. P., Bochanski, J. J., et al. 2011, AJ, 141, 97, doi: [10.1088/0004-6256/141/3/97](https://doi.org/10.1088/0004-6256/141/3/97)
- Yang, H., Liu, J., Gao, Q., et al. 2017, ApJ, 849, 36, doi: [10.3847/1538-4357/aa8ea2](https://doi.org/10.3847/1538-4357/aa8ea2)
- Zechmeister, M., & Kürster, M. 2009, A&A, 496, 577, doi: [10.1051/0004-6361:200811296](https://doi.org/10.1051/0004-6361/200811296)